Test rig with active damping control for the simultaneous evaluation of vibration control and energy harvesting via piezoelectric transducers

S Perfetto[1], J Rohlfing[1,2], F Infante[1], D Mayer[1] and S Herold[1]

[1]Fraunhofer Institute for Structural Durability and System Reliability LBF, Darmstadt, Germany
[2]Research Group of System Reliability and Machine Acoustics SzM, Technical University Darmstadt, Darmstadt, Germany

E-mail: sara.perfetto@lbf.fraunhofer.de

Abstract. Piezoelectric transducers can be used to harvest electrical energy from structural vibrations in order to power continuously operating condition monitoring systems local to where they operate. However, excessive vibrations can compromise the safe operation of mechanical systems. Therefore, absorbers are commonly used to control vibrations. With an integrated device, the mechanical energy that otherwise would be dissipated can be converted via piezoelectric transducers. Vibration absorbers are designed to have high damping factors. Hence, the integration of transducers would lead to a low energy conversion. Efficient energy harvesters usually have low damping capabilities; therefore, they are not effective for vibration suppression. Thus, the design of an integrated device needs to consider the two conflicting requirements on the damping. This study focuses on the development of a laboratory test rig with a host structure and a vibration absorber with tunable damping via an active relative velocity feedback. A voice coil actuator is used for this purpose. To overcome the passive damping effects of the back electromagnetic force a novel voltage feedback control is proposed, which has been validated both in simulation and experimentally. The aim of this study is to have a test rig ready for the introduction of piezo-transducers and available for future experimental evaluations of the damping effect on the effectiveness of vibration reduction and energy harvesting efficiency.

1. Introduction

Wireless sensors and data transmission are important elements in health condition monitoring systems. With the advent of smart structures, the demand for wireless sensors has increased. Currently most of such sensors require a periodic battery replacement. This can be solved by using the electric energy harvested directly where and when the sensors operate. Thus, maintenance times and costs can be reduced. At present, the most available vibration-to-electric conversion mechanisms are based on electrostatic, electromagnetic and piezoelectric transducers. Among these three types, those based on piezoelectric materials are often preferable because the energy density that can be harvested is three times higher than for other transducer principles [1]. This justifies the choice of using piezo ceramics to convert the energy. The most simple piezo transducers are piezo-patches, which are glued directly on a structure and connected to an electric circuit. The design of the mechanical system is of crucial

importance for the efficiency of the energy harvester. For instance, the electrical power that can be harvested decreases when a structure is strongly damped [2].

On the other hand excessive vibrations affect the normal operation of mechanical systems like civil, aerospace and automotive structures or industrial machine tools. Traditionally passive methods are used to control structural vibrations and extensive studies have been carried out on this topic [3]. A common approach is that of tuned vibration absorbers (TVAs), which are single degree of freedom systems mounted on a structure and tuned to the same natural frequency. The value of the mechanical parameters such as mass and stiffness are of primary importance and the choice of the damping is crucial. Formulas for computing optimal damping factors are suggested in literature and their values are usually quite high (15% - 25%). A basic vibration absorber can be composed of a mass coupled to the vibrating structure via an elastic connection, for example by a cantilever beam. Such a structure can be adapted to be used for energy harvesting if the beam host the piezoelectric transducers. For this reason the study of an integrated device as energy harvesting vibration absorber (EHVA) is very attractive. Analytical studies have shown that some requirements, for example those on the optimal damping or on the optimal mass ratio for the two tasks, are conflicting and need to be investigated carefully [4,5].

Usually, TVAs are designed to have high damping factors. Thus, the integration of piezoelectric transducers in a prior designed absorber would lead to a low efficient energy harvester. On the other hand, in fact, the devices used for energy conversion are characterized by low damping values, which are often not effective for vibration suppression. Therefore, the design of an EHVA needs to take into account the two conflicting requirements on the damping.

In order to simultaneously evaluate the effect of the absorber damping on vibration reduction and electric power generation, a simulation model of an EHVA has been implemented. To validate this model experimentally, a test rig has been developed. The aim of the test rig is then to validate the model of the EHVA in various conditions of damping. Before the introduction of piezo-transducers, not discussed in this paper, a method for varying the damping factor of the absorber has been investigated. The set-up is composed by a host structure, which represents a single degree of freedom system mounted on a structure characterized by infinite impedance, and a TVA attached to it. The absorber in constructed from a metal beam, which will allow the installation of piezoelectric transducers for the evaluation of energy harvesting capabilities, and an end mass. Usually metals have very low structural damping. An increase in the damping of a metal beam can be achieved by applying layers of viscoelastic materials or, more efficiently, by using constrained layer damping (CLD). It is also possible to exploit electromagnetic effects to create damping. The main advantage is that damping is added without coming into contact with the structure. The passive electromagnetic damper functions due to the eddy currents induced by the motion of a conductor in a static magnetic field and it was investigated first by Sodano [6-9]. Bea et al. have studied intensively the case of a passive TVA where an eddy current damper is used [10,11]. Nevertheless, variable damping over a wide range of damping ratios is hard to achieve passively. With the advances in technology, semi-active and active controls have also become available. The semi-active systems improve the passive damper by allowing the magnet´s position to be actively controlled. The active systems, like voice coil actuators (VCAs), allow actively modifying the current flowing in the coil via a velocity feedback, thus generating a damping effect. They can be current driven or voltage driven and, usually, the feedback controls are built with an absolute velocity. However, in the case of damping between the mass of the primary structure and the absorber mass, a relative velocity feedback has to be used to represent the realistic damping element. To be noticed is that other active control systems are available for this purpose, for example those that involve piezo transducers, but these controls may not be suitable due to the small forces generated.

Thus, a voice coil actuator has been introduced in the test rig described before, with the aim of studying (after the introduction of the transducers) the behavior of the EHVA for damping factors in the range of almost zero damping to over critical values; the magnet has been used as absorber mass while the coil is attached to the host structure. By controlling the current/voltage flowing in the coil,

the damping of the absorber can be manipulated. Two relative velocity feedback controls have been implemented for the two cases of current driven actuator and voltage driven actuator.

After an introduction concerning the model used to describe the global system (section 2), the analytical formulations of the feedback controls are discussed in sections 3 and 4. The experimental setup is described in section 5 and the limits of such controls are discussed. To overcome the passive effect of the back electromagnetic force, a novel voltage feedback control is proposed in section 6 and it has been validated experimentally and in simulations. The results obtained with such control are discussed. The test rig is now available for further experimental investigations, to which an outlook is given in the last section.

2. Model of a vibration absorber with a VCA

The test rig can be represented by a two degrees of freedom (2DoF) mass-spring-damper system. The host structure, with mass m_{H}, is bounded to a fixed support by elastic connections represented by total stiffness k_{H} and damping c_{H}. This structure is excited by an external source (F_{ext}). A TVA is attached to it and is composed by a suspension with stiffness k_{a} and damping c_{a}, and a tip mass m_{a}. To adjust the damping of the absorber, a VCA is inserted between the host structure and the absorber.

To describe the whole system, the impedance formulation has been chosen [12]. The actuator can be modelled using its electrical impedance, in order to have a concise formulation of the overall system. The VCA is represented by the inductance $\mathrm{L_e}$ and the resistance $\mathrm{R_e}$ of the coil and by the force constant Ψ [N/A]. The coil is powered by a feedback signal generated through the relative velocity (between host mass and absorber mass) and a gain $\hat{g}$.

In figure 1(a) a framework of the system is shown and in figure 1(b) the notations used for the forces acting on the two masses are depicted.

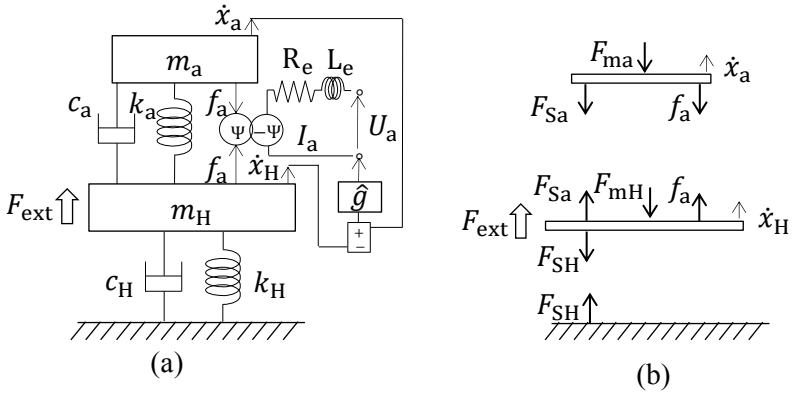

Figure 1. Framework of the 2DoF system with VCA and relative velocity feedback (a) - Reactions on the system (b)

The force acting on the host mass is $F_{\mathrm{mH}} = Z_{\mathrm{mH}}\dot{x}_{\mathrm{H}}$ where $Z_{\mathrm{mH}} = \mathrm{i}\omega m_{\mathrm{H}}$ is the impedance of the host mass and $\dot{x}_{\mathrm{H}}$ is its velocity. Similarly, the force acting on the absorber mass is $F_{\mathrm{ma}} = Z_{\mathrm{ma}}\dot{x}_{\mathrm{a}}$ where $Z_{\mathrm{ma}} = \mathrm{i}\omega m_{\mathrm{a}}$ is the impedance of the secondary mass and $\dot{x}_{\mathrm{a}}$ is the correspondent velocity. The reaction due to spring and damper between the two masses is $F_{\mathrm{Sa}} = Z_{\mathrm{Sa}}(\dot{x}_{\mathrm{a}} - \dot{x}_{\mathrm{H}})$, where $Z_{\mathrm{Sa}} = c_{\mathrm{a}} + k_{\mathrm{a}}/\mathrm{i}\omega$ is the corresponding mechanical impedance. The reaction due to spring and damper of the host structure is defined as $F_{\mathrm{SH}} = Z_{\mathrm{SH}}(\dot{x}_{\mathrm{H}})$, where $Z_{\mathrm{SH}} = c_{\mathrm{H}} + k_{\mathrm{H}}/\mathrm{i}\omega$ is the corresponding mechanical impedance. The actuation force is indicated with f_{a}. Its definition depends on the kind of feedback and will be described in the next sections. The impedance of the total system is $Z_{\mathrm{TOT}} = F_{\mathrm{ext}}/\dot{x}_{\mathrm{H}}$ and it changes for different feedback control settings. The admittance, as consequence, is defined as the inverse of the total impedance.

The force balances on the host mass and on the secondary mass are the followings:

$$F_{\mathrm{mH}} + F_{\mathrm{SH}} - F_{\mathrm{Sa}} - f_{\mathrm{a}} = F_{\mathrm{ext}}, \tag{1}$$

$$F_{\mathrm{ma}} + F_{\mathrm{Sa}} + f_{\mathrm{a}} = 0. \tag{2}$$

3. Current driven feedback control actuator

This section provides a mathematical derivation of the impedance Z_{TOT} of the global system when a current proportional to the relative velocity is used to drive the actuator. In this case the control force directly results from Lorentz law, which states that the force f_{a} generated by a wire carrying an electrical current within a magnetic field is given by

$$f_{\mathrm{a}} = BlI_{\mathrm{a}} = \Psi I_{\mathrm{a}}, \tag{3}$$

where B is the magnetic flux density and l denotes the length of the coil exposed to the magnetic flux. Both factors are combined to a transducer force constant Ψ with dimension $[\mathrm{N/A}]$. For a current controlled feedback signal to the actuator, the current I_{a} is given by

$$I_{\mathrm{a}} = \hat{g}(\dot{x}_{\mathrm{a}} - \dot{x}_{\mathrm{H}}), \tag{4}$$

which gives the control force as

$$f_{\mathrm{a}} = \Psi\hat{g}(\dot{x}_{\mathrm{a}} - \dot{x}_{\mathrm{H}}). \tag{5}$$

The total gain used to build the feedback control is $\hat{g} = Gg$, where G denotes the gain of the amplifier necessary to power the coil and g is the feedback gain varied to modify the damping of the absorber. As consequence, the frequency response function (FRF) of $\dot{x}_{\mathrm{a}}/\dot{x}_{\mathrm{H}}$ and the total admittance of the system are described in equations (6) and (7) respectively.

$$\frac{\dot{x}_{\mathrm{a}}}{\dot{x}_{\mathrm{H}}} = \frac{Z_{\mathrm{Sa}} + Gg\Psi}{Z_{\mathrm{ma}} + Z_{\mathrm{Sa}} + Gg\Psi}, \tag{6}$$

$$\frac{\dot{x}_{\mathrm{H}}}{F_{\mathrm{ext}}} = \frac{1}{Z_{\mathrm{mH}} + Z_{\mathrm{SH}} + \dfrac{Z_{\mathrm{ma}}(Z_{\mathrm{Sa}} + Gg\Psi)}{Z_{\mathrm{ma}} + Z_{\mathrm{Sa}} + Gg\Psi}}. \tag{7}$$

The FRFs of $f_{\mathrm{a}}/(\dot{x}_{\mathrm{a}} - \dot{x}_{\mathrm{H}})$ and of $\dot{x}_{\mathrm{a}}/\dot{x}_{\mathrm{H}}$ are represented in figures 2 and 3 respectively for $\hat{g} = 1$.
The contribution to the total impedance given by the term $Z_{\mathrm{I}} = \frac{Z_{\mathrm{ma}}(Z_{\mathrm{Sa}}+Gg\Psi)}{Z_{\mathrm{ma}}+(Z_{\mathrm{Sa}}+Gg\Psi)}$ represents the impedance due to mass, stiffness and damping of the absorber and to the actuation force. It can also be seen as the impedance $Z_{\mathrm{I}} = \frac{m_{\mathrm{a}}\ddot{x}_{\mathrm{a}}}{\dot{x}_{\mathrm{H}}}$ and denotes two different contributions:

- an active contribution that depends on the amplifier and the feedback gains and on the force constant:

$$Z_{\mathrm{ACT_I}} = Gg\Psi\left(\frac{Z_{\mathrm{ma}}}{Z_{\mathrm{ma}} + Z_{\mathrm{Sa}}}\right)\left(1 - \frac{\dot{x}_{\mathrm{a}}}{\dot{x}_{\mathrm{H}}}\right), \tag{8}$$

  it can be seen as the difference between the actuator impedance calculated when the feedback is built using only $\dot{x}_{\mathrm{H}}$ and that calculated when the feedback uses only $\dot{x}_{\mathrm{a}}$;
- a passive contribution that depends only on mechanical parameters, but not on gains:

$$Z_{\mathrm{PASS_I}} = \frac{Z_{\mathrm{ma}}Z_{\mathrm{Sa}}}{Z_{\mathrm{ma}} + Z_{\mathrm{Sa}}}, \tag{9}$$

and it is $Z_{\mathrm{ACT_I}} + Z_{\mathrm{PASS_I}} = \mathrm{Z_I}$. The damping force produced by the VCA is proportional to the gain. Theoretically, when the feedback gain (or the amplifier gain) is zero, such force is zero and no current

is flowing in the coil. However, there is an effect that is not considered in the model: the interaction between magnet and coil generates an electromagnetic effect and, thus, an additional damping even if the coil is not connected to the amplifier. In addition, a very small air gap separates the coil from the magnet and they cannot move really freely one respect to the other. The prediction of these damping effects is very complex. As an alternative to adjust the mathematical model, they could be measured and collected in a new damping term D that modifies the impedance in $Z_{\mathrm{Sa}} = c_{\mathrm{a}} + D + k_{\mathrm{a}}/\mathrm{i}\omega$.

4. Voltage driven feedback control actuator

Typically, voice coil actuators are powered by amplifiers that provide an input proportional output voltage signal. For a voltage controlled feedback signal, the control voltage U_{a} is given by

$$U_{\mathrm{a}} = \hat{g}(\dot{x}_{\mathrm{a}} - \dot{x}_{\mathrm{H}}), \tag{10}$$

where $\hat{g} = Gg$, as defined before. The electro-mechanical coupling follows from Faraday´s law, which states that the moving coil generates voltage. This induced voltage is given by

$$U_{\mathrm{ind}} = \Psi(\dot{x}_{\mathrm{H}} - \dot{x}_{\mathrm{a}}). \tag{11}$$

The electrical subsystem is described by the differential equation

$$\mathrm{R_e} I_{\mathrm{a}} + \mathrm{L_e}\frac{\mathrm{d}I_{\mathrm{a}}}{\mathrm{d}t} + U_{\mathrm{ind}} = U_{\mathrm{a}}, \tag{12}$$

where $\mathrm{R_e}$ and $\mathrm{L_e}$ are the resistance and the inductance of the coil respectively. Equations (10), (11) and (12) allow the calculation of the current I_{a}, necessary for the estimation of the actuator force f_{a} by equation (3). The current is computed as

$$I_{\mathrm{a}} = \frac{U_{\mathrm{a}}}{Z_{\mathrm{e}}} - \frac{\Psi}{Z_{\mathrm{e}}}(\dot{x}_{\mathrm{H}} - \dot{x}_{\mathrm{a}}) = \frac{(\hat{g} + \Psi)}{Z_{\mathrm{e}}}(\dot{x}_{\mathrm{a}} - \dot{x}_{\mathrm{H}}), \tag{13}$$

where $Z_{\mathrm{e}} = \mathrm{R_e} + \mathrm{i}\omega\mathrm{L_e}$ is the electrical impedance of the VCA. Thus, the force becomes

$$f_{\mathrm{a}} = \frac{\Psi}{Z_{\mathrm{e}}}(\hat{g} + \Psi)(\dot{x}_{\mathrm{a}} - \dot{x}_{\mathrm{H}}). \tag{14}$$

As consequence, the FRF of $\dot{x}_{\mathrm{a}}/\dot{x}_{\mathrm{H}}$ and the admittance of the global system are described in equations (15) and (16) respectively.

$$\frac{\dot{x}_{\mathrm{a}}}{\dot{x}_{\mathrm{H}}} = \frac{Z_{\mathrm{Sa}} + \frac{\Psi}{Z_{\mathrm{e}}}(Gg + \Psi)}{Z_{\mathrm{ma}} + Z_{\mathrm{Sa}} + \frac{\Psi}{Z_{\mathrm{e}}}(Gg + \Psi)}, \tag{15}$$

$$\frac{\dot{x}_{\mathrm{H}}}{F_{\mathrm{ext}}} = \frac{1}{Z_{\mathrm{mH}} + Z_{\mathrm{SH}} + \frac{Z_{\mathrm{ma}}\left[Z_{\mathrm{Sa}} + \frac{\Psi}{Z_{\mathrm{e}}}(Gg + \Psi)\right]}{Z_{\mathrm{ma}} + Z_{\mathrm{Sa}} + \frac{\Psi}{Z_{\mathrm{e}}}(Gg + \Psi)}}. \tag{16}$$

Figures 2 and 3 show the comparison between the FRFs of $f_{\mathrm{a}}/(\dot{x}_{\mathrm{a}} - \dot{x}_{\mathrm{H}})$ for current and voltage controlled feedback from equations (5) and (14) and the FRFs of $\dot{x}_{\mathrm{a}}/\dot{x}_{\mathrm{H}}$ from equations (6) and (15) respectively. The peaks correspond to the natural frequency of the absorber at ~37 Hz and a gain $\hat{g} = 1$ is used as example. In case of voltage feedback, the $f_{\mathrm{a}}/(\dot{x}_{\mathrm{a}} - \dot{x}_{\mathrm{H}})$ decreases when the frequency increases while with current feedback it remains constant. As in the case of current feedback, the contribution to the total impedance given by the term $Z_{\mathrm{U}} = \frac{Z_{\mathrm{ma}}\left[Z_{\mathrm{Sa}} + \frac{\Psi}{Z_{\mathrm{e}}}(Gg + \Psi)\right]}{Z_{\mathrm{ma}} + Z_{\mathrm{Sa}} + \frac{\Psi}{Z_{\mathrm{e}}}(Gg + \Psi)}$ represents

the impedance due to mass, stiffness and damping of the absorber and to the actuation force. It denotes two different contributions:

- an active contribution that depends on the amplifier and feedback gains and on the force constant:

$$Z_{\mathrm{ACT_U}} = Gg\frac{\Psi}{Z_{\mathrm{e}}}\left(\frac{Z_{\mathrm{ma}}}{Z_{\mathrm{ma}} + Z_{\mathrm{Sa}} + \frac{\Psi^2}{Z_{\mathrm{e}}}}\right)\left(1 - \frac{\dot{x}_{\mathrm{a}}}{\dot{x}_{\mathrm{H}}}\right), \tag{17}$$

  as before, it can be seen as the difference between the actuator impedance calculated when the feedback is built using only $\dot{x}_{\mathrm{H}}$ and that calculated when the feedback uses only $\dot{x}_{\mathrm{a}}$;
- a passive contribution that depends in this case on mechanical parameters and also on the force constant, but still not on gains:

$$Z_{\mathrm{PASS_U}} = \frac{Z_{\mathrm{ma}}\left(Z_{\mathrm{Sa}} + \frac{\Psi^2}{Z_{\mathrm{e}}}\right)}{Z_{\mathrm{ma}} + Z_{\mathrm{Sa}} + \frac{\Psi^2}{Z_{\mathrm{e}}}}. \tag{18}$$

Again, it is $Z_{\mathrm{ACT_U}} + Z_{\mathrm{PASS_U}} = Z_{\mathrm{U}}$. Moreover, to be noted from equations (10) and (13) is that when the feedback gain g (or the amplifier gain G) is zero, it is $U_{\mathrm{a}} = 0$ but $I_{\mathrm{a}} \neq 0$. Thus, from equation (12), there is an induced voltage in the wire and, as consequence, an actuation force. Thus, besides the electromagnetic damping effects (D) mentioned before and still present in this case, when the voltage feedback is used, there is also a passive damping effect due to the back electromagnetic force (back emf) proportional to Ψ^2/Z_{e}. Such term is predominant respect to D and does not depend on the gains. Negative values of g allow reducing the back emf but, by increasing its value, the system becomes unstable before reaching the original structural damping. Thus, the control of the damping with a simple voltage feedback is inaccurate and it is not possible to cover the damping range from 0 to over critical values. This highlights the necessity to develop a new feedback control law considering the specific dynamic characteristics of a voltage controlled VCA.

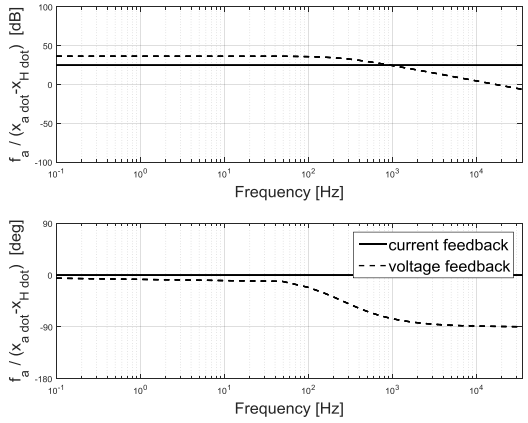

Figure 2. FRFs of $f_{\mathrm{a}}/(\dot{x}_{\mathrm{a}} - \dot{x}_{\mathrm{H}})$ over frequency for current and voltage driven control force ($\hat{g} = 1$)

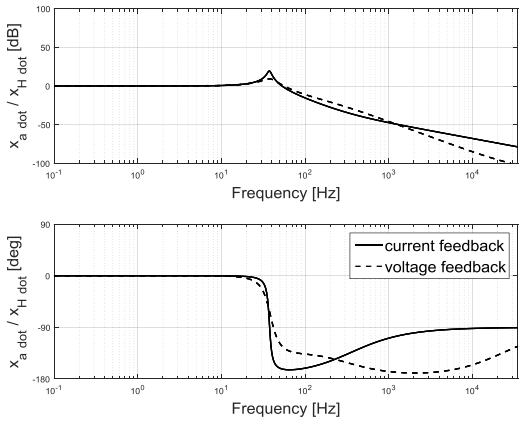

Figure 3. FRFs of $\dot{x}_{\mathrm{a}}/\dot{x}_{\mathrm{H}}$ over frequency for current and voltage driven feedback controls ($\hat{g} = 1$)

5. Experimental setup and validations

The test rig consists of a primary structure, named as host structure, and a secondary structure that acts as TVA for the host. The mass of the host structure is represented by m_{H} in the 2DoF framework discussed in section 2. It has been realized in aluminium due to the necessity of making its dimensions sufficiently big to allow allocating the VCA between the host structure and the TVA, without

increasing excessively the weight. In addition, it is not magnetic. Since the actuator chosen is composed by a heavy magnet and a light coil, the magnet itself acts as the mass of the absorber m_a. The host mass has been designed to give a mass ratio $\mu = m_a/m_H$ in the optimal range $(0.1 - 0.2)$ for vibration reduction [3]. The host mass is connected to a fixed support through two steel beams, represented in figure 1 by their combined stiffness k_H and damping c_H. The host structure can move only in the direction of the excitation and can therefore be modelled as a single degree of freedom system. Its natural frequency has been simulated and measured as ~ 41 Hz. In similar way, the absorber is assumed to be a one degree of freedom mass-spring-damper system. The magnet is connected to the host structure via a stainless steel beam, characterized by stiffness k_a and damping c_a. The tuning frequency of the absorber, optimal for vibration reduction, has been calculated following the Den Hartog´s theory and it has been simulated and measured as ~ 37 Hz. The actuator used in the experimental setup is the model VLR0113-0089-00A provided by Willburger System GmbH and its characteristics are summarized in table 1.

Table 1. Parameters of the VCA

Peak force[a] F_p [N]	Continuous Force[b] [N]	Total stroke [mm]	Mass of coil [g]	Mass of magnet [g]
113	35	8.9	130	470

Force constant Ψ [N/A]	Resistance R_e[Ohm]	Inductance L_e[mH]	Current[c] @ F_p [A]	Voltage[c] @ F_p [V]
17.5	4.8	3.0	6.5	31

[a]10 sec @ 25 °C ambient, 150 °C coil temperature, [b] 5 °C ambient, 150 °C coil temperature, [c]Nominal

The measurements have been conducted with a PCB 086C02 modal hammer (averaged over 10 measurements) and with a TIRA shaker TV 50018, both not represented in figure 4. The accelerations of the host mass and of the absorber mass have been measured using two PCB 352C33 accelerometers.

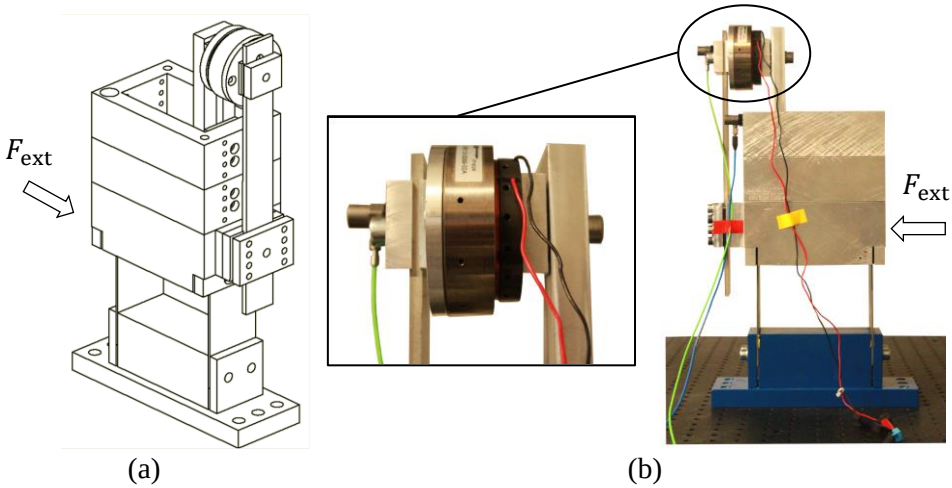

Figure 4. Complete test rig: CAD model (a) and experimental setup (b)

Figure 5 shows the results from the finite element analysis for the first (a) and the second (b) vibration modes of the combined host-absorber structure. As mentioned before, the host structure can only move in the direction of the applied force, acting like a single degree of freedom system. Similar behaviour

can be detected looking at the absorber: its motion is in phase with the host (first mode) or out of phase (second mode).

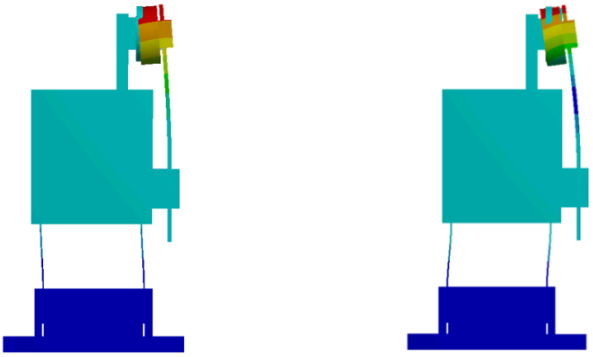

(a) (b)

Figure 5. First (a) and second (b) vibration modes of the FE model

5.1 Measurements and simulations with current and voltage feedback controls

For both feedback controls described in sections 3 and 4, MATLAB/Simulink models have been implemented, together with analytical formulations based on the impedance model described in section 2. In the following, measurements and simulations of the admittance $\dot{x}_{\mathrm{H}}/F_{\mathrm{ext}}$ over frequency are shown. Three feedback gains are used as example: $g = 0$, $g = 0.25$ and $g = 0.5$ and an amplifier gain $G \approx 6$. For the experimental studies the feedback control loops have been implemented on a dSpace system running at a sample rate of $2^{14}\ Hz$. This high sampling rate is necessary to minimize delays due to the digital system.

Figure 6 shows the results of measurements and simulations of the FRF expressed in equation (7) for various values of feedback gain when a current feedback is used. When $g = 0$, the only additional contribution to the structural damping is that due to the electromagnetic effect (D) and it is not negligible compared to the pure mechanical one.

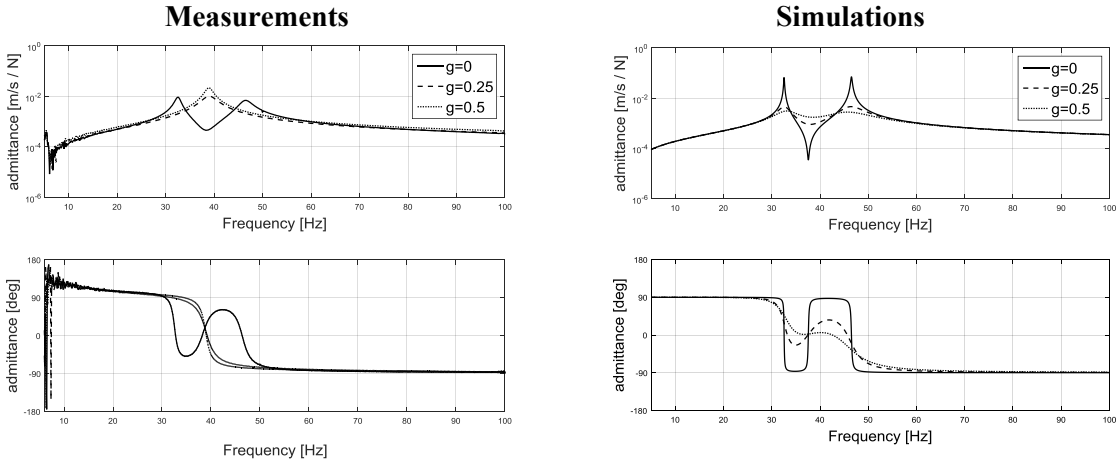

Figure 6. Measurements and simulations with relative velocity current feedback

As anticipated in section 3, this effect is not considered in the simulation because a complex mathematical model would be required to properly represent it. As consequence, by increasing the gain from $g = 0$ to $g = 0.5$, different results are found during the measurements because the real damping is much higher. In conclusion, the simulation model with current feedback is not accurate in the prediction of the real behaviour of the system.

Figure 7 shows the results for the voltage driven velocity feedback. The simulations are based on equation (16) in section 4. As expected, when the gain is zero a strong effect of passive damping is registered due to the back emf term Ψ^2/Z_e and, because it is considered in the mathematical model, it is visible both in the measurements and in the simulations. This effect is very strong due to the high force constant of the actuator used. It adds up with the damping D due to the electromagnetic effect and dominates the overall damping of the system. Also, the influence of changes of the feedback gain on the dynamics of the system is minimal. The gain of the amplifier is still $G \approx 6$. In this case, the simulation model with voltage feedback is able to predict the behaviour of the system with sufficient accuracy. However, the control of the damping is not possible since the passive system with short circuited VCA is already highly damped. Therefore, in order to power the coil with the voltage and to control the damping of the system, a new voltage feedback has been developed.

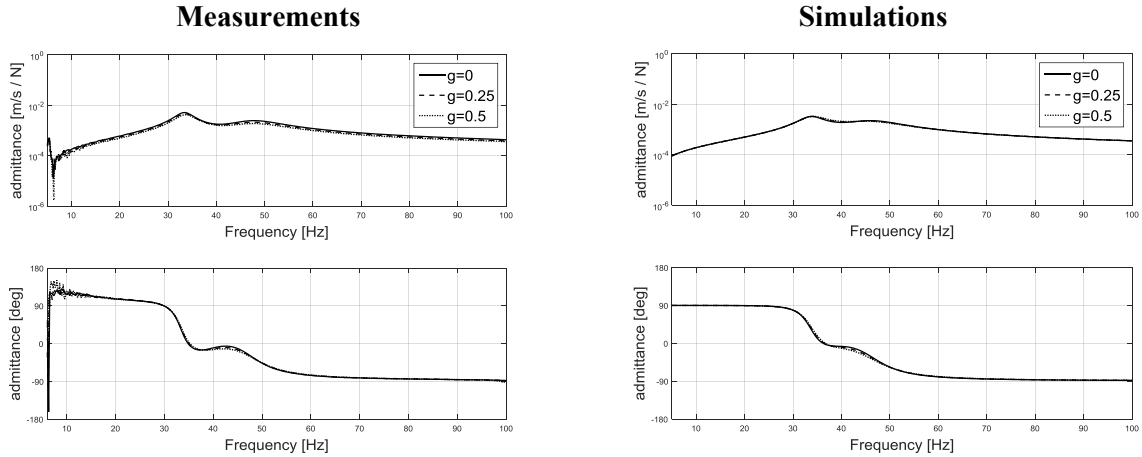

Figure 7. Measurements and simulations with relative velocity voltage feedback

As can be observed in the figures above, both with the current and with the voltage feedback controls presented it is not possible to achieve the low damping factors desired for the experiment.

6. Novel voltage driven feedback control actuator

In the previous sections it has been demonstrated that simple current driven and voltage driven velocity feedback are not suitable for a correct and easy control of the damping of the structure: in a system with current feedback there are strong electromagnetic damping effects and in a system with voltage feedback, in addition, there is a high damping due to the back emf that cannot be controlled or cancelled easily, since it does not depend on control and amplifier gains. To overcome this problem, a novel voltage feedback control with a regulator has been developed and validated both in simulation and experimentally. The method applies a new feedback gain g^* which is a function of the feedback control gain g and a regulator gain g_2:

$$g^* = g\, C_1 + g_2\, C_2 \tag{19}$$

where C_1, C_2 and g_2 are system specific terms that need to be determined. Thus, the total gain is $\hat{g} = G g^*$and the architecture of the system in Figure 1 has not changed except for the new gain. Similarly, equations (10)-(18) are unchanged provided that g is replaced by g^*.

To cancel the effect of the passive damping, the choice of the values is immediate: $C_1 = Z_e$ and $C_2 = -\Psi$. As consequence, equations (14) and (16) can be rewritten as follows:

$$f_a = \frac{\Psi}{Z_e}[G(gZ_e - g_2\Psi) + \Psi](\dot{x}_a - \dot{x}_H) \tag{20}$$

$$\frac{\dot{x}_{\mathrm{H}}}{F_{\mathrm{ext}}} = \frac{1}{Z_{\mathrm{mH}} + Z_{\mathrm{SH}} + \dfrac{Z_{\mathrm{ma}}\left\{Z_{\mathrm{Sa}} + \dfrac{\Psi}{Z_{\mathrm{e}}}[G(gZ_{\mathrm{e}} - g_2\Psi) + \Psi]\right\}}{Z_{\mathrm{ma}} + Z_{\mathrm{Sa}} + \dfrac{\Psi}{Z_{\mathrm{e}}}[G(gZ_{\mathrm{e}} - g_2\Psi) + \Psi]}} \tag{21}$$

where the contribution to the total impedance given by the term $Z_{\mathrm{U}^*} = \frac{Z_{\mathrm{ma}}\left\{Z_{\mathrm{Sa}}+\frac{\Psi}{Z_{\mathrm{e}}}[G(gZ_{\mathrm{e}}-g_2\Psi)+\Psi]\right\}}{Z_{\mathrm{ma}}+Z_{\mathrm{Sa}}+\frac{\Psi}{Z_{\mathrm{e}}}[G(gZ_{\mathrm{e}}-g_2\Psi)+\Psi]}$ represents the impedance due to mass, stiffness and damping of the absorber and to the actuator, as before.

If $Gg_2 = 1$, equations (20) and (21) become equations (5) and (7) respectively. In this way, the actuator force is again directly proportional to the relative velocity by the total gain ΨGg and the system with voltage feedback behaves as that with current feedback. The choice of the amplifier gain G is arbitrary and, during the experiments, it is difficult to accurately identify its actual numerical value. However, for an arbitrary value of G, the gain g_2 can be easily selected during the experiment by adjusting the system to give close to zero damping in order to satisfy the $g_2 = 1/G$. This provides not only $f_{\mathrm{a}} = 0$ when $g = 0$ (no effects due to back emf) but also allows to cancel the electromagnetic damping D, that is not considered in the mathematical model. This last consideration provides an improvement respect to the case of current feedback presented. To be noticed is that, when the actuator is driven by a current signal, a new regulator could be used to take into account the measured electromagnetic damping effects. This solution would probably be equivalent to that presented in this section but it has not been further investigated.

6.1 Measurements and simulations with regulated voltage feedback control

The experimental setup described in section 5 is used to validate the new voltage feedback control. The regulator has been implemented in MATLAB/Simulink (figure 8) as also the complete simulation model. The measurements in real time have been executed via a dSpace system running at a sample rate of 2^{14} Hz. As mentioned before, the value of g_2 is easily chosen manually during the measurements: once the gain of the amplifier is fixed, g_2 is the minimum value that produces a close to zero damping, yet does not drive the system unstable.

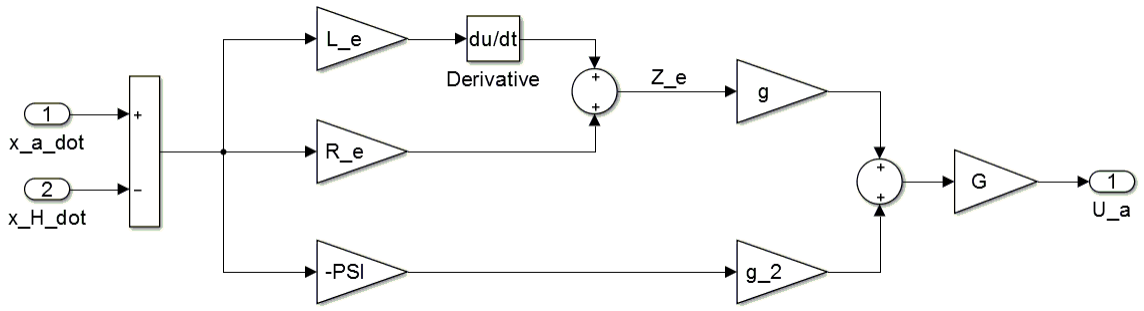

Figure 8. Regulator for voltage feedback control

When g_2 is identified, also the value of G becomes known by $G \approx 1/g_2$. Figure 9 shows the results of measurements and simulations for different values of feedback gain ($g = 0, g = 0.25, g = 0.5$) in the case of $g_2 = 0.165$ (with $G \approx 6$). The model appears now suitable to predict the behaviour of the system. In particular, when $g = 0$, the system behaves as without coil: the measurements obtained on the test rig in this case correspond to the simulations of the 2DoF system when the coil is removed. This demonstrates that the regulated voltage feedback control is able not only to overcome the passive damping effects of the back emf but also those due to the electromagnetic damping and small air gap. When the gain increases, the model gives sufficient accurate results.

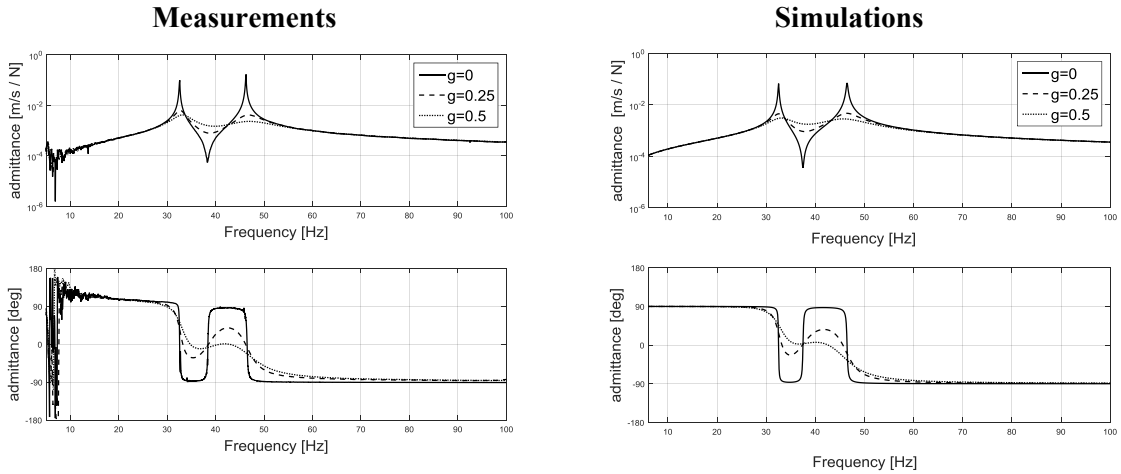

Figure 9. Measurements and simulations with novel relative velocity voltage feedback

6.2 Estimation of the gain for the desired damping factor

With reference to the impedance Z_{U^*}, when $Gg_2 = 1$ the contribution of absorber damping is collected in terms like $(Z_{Sa} + GgΨ)$, where $Z_{Sa} = c_a + k_a/i\omega$ represents the impedance due to structural stiffness and damping of the absorber. Thus, the impedance related to the damping can be defined as $Z_{Da} = c_a + GgΨ$. As consequence, the damping ratio of the absorber $\xi_{a\,TOT}$ can be seen as the sum of the mechanical ratio ξ_a and the additional ratio due to the actuator. From this result, the gain g necessary to provide the desired $\xi_{a\,TOT}$ can be easily computed as

$$g = \frac{2\xi_{\mathrm{a\,TOT}}\sqrt{m_{\mathrm{a}}k_{\mathrm{a}}} - c_{\mathrm{a}}}{G\Psi}. \tag{22}$$

The absorber built with the stainless steel beam presented an initial damping factor $\xi_{\mathrm{a}} \approx 0.3\%$. The use of $g_2 = 0.165$ and $g = 0$, $g = 0.25$ and $g = 0.5$ has provided total damping factors of $\xi_{\mathrm{a\,TOT}} \approx 0.3\%$, $\xi_{\mathrm{a\,TOT}} \approx 8\%$ and $\xi_{\mathrm{a\,TOT}} \approx 15.6\%$ respectively. Thus, the increase of the damping factor in the experiment is almost linear with the gain, which is in good agreement with the formulation in equation (22). An additional test has been conducted for $g = 0.67$ and $\xi_{\mathrm{a\,TOT}} \approx 21\%$. Once the transducers will be integrated into the TVA, an additional damping effect will have to be considered. For instance, if a pure resistive circuit (R_{ext}) is connected to them, the impedance related to the damping becomes $Z_{Da} = c_a + GgΨ + \vartheta^2 Z_p$ where ϑ is the electromechanical damping factor and $Z_p = R_{ext}/(j\omega R_{ext} C_p + 1)$, with C_p capacitance of the transducers. Since the coupling factor is usually $\vartheta^2 \ll 1$, the additional effect is often not strongly influent. However, different considerations in this regard could be done by improving the electric circuit connected to the energy harvester.

7. Conclusions and outlook

To simultaneously evaluate vibration reduction and energy harvesting capabilities of an EHVA, a test rig has been designed and built to validate the simulation model. Since usually metals have very low damping capabilities, a method to control the damping of the TVA has been investigated before the introduction of piezoelectric transducers. This allows carrying out an experimental validation of the EHVA behaviour in various damping conditions.

This paper presents the results of experimental and simulation studies on control feedback strategies for eddy current dampers. Both current and voltage relative velocity feedback controls have been investigated. The limits of the models used in the simulations have been shown: the inaccuracy in

the prediction of the electromagnetic effect causes unexpected damping factors. Such effect is clearly visible when a current feedback is used. In case of voltage feedback, an additional damping effect due to the back electromagnetic force does not allow to observe the behaviour of the system with original (almost zero) damping. To overcome these limits, a novel relative velocity voltage feedback control has been developed: a regulator allows not only to minimize the passive damping effect due to the back emf but also to compensate the effects of electromagnetic damping. In this way, it has been demonstrated that the damping of the absorber becomes proportional to the feedback gain and can be predicted with sufficient accuracy. Thus, the value of gain necessary to have a desired damping factor can be computed. As consequence, the damping of the TVA can be varied in the range from zero to over critical values, in order to study its influence on the dynamics of the system.

Because the behaviour of such a device as energy harvester is also strongly influenced by damping, after the introduction of piezo-patches the set-up will allow to simultaneously evaluate the effects of mechanical damping on the effectiveness of the integrated device in terms of both vibration reduction and energy harvested. The VCA and the relative velocity control law discussed in this paper will be used to vary the damping of the absorber in a defined manner. More work is now in progress to investigate the effectiveness of vibration reduction and energy harvesting efficiency with various damping factors.

References

[1] Priya S 2007 Advances in energy harvesting using low profile piezoelectric transducers *J. Electroceram.* **19** pp 165-182
[2] Priya S and Inman D J 2009 *Energy Harvesting Technologies* (Springer Editor)
[3] Den Hartog J P 1956 *Mechanical Vibrations* (4th Edition McGraw-Hill Editor)
[4] Perfetto S et al. 2014 Feasibility study of an anenergy harveting system integrated with a rotational vibration absorber *Proc. Int. Conf. on Noise and Vibration Engineering ISMA (Leuven, Belgium)*
[5] Perfetto S et al. 2015 An analytical model of a piezoelectric energy harvesting device integrated with a rotational vibration absorber *Proc. Int. Conf. on Noise and Vibration Emerging Technologies NOVEM (Dubrovnik, Croatia)*
[6] Sodano H A 2005 *Development of Novel Eddy Current Dampers for the Suppression of Structural Vibrations* (PhD Dissertation: Virginia Polytechnic Institute and State University)
[7] Sodano H A, Bae J and Inman D J 2005 Concept and model of eddy current damper for vibration suppression of a beam *J. of Sound and Vibration* **288** Issues 4-5 pp 1177-1196
[8] Sodano H A, Bae J and Inman D J 2006 Modeling and application of eddy current damper for suppression of membrane vibrations *AIAA Journal* **44** Issue 3 pp 541-549
[9] Sodano H A, Bae J and Inman D J 2006 Improved concept and model of eddy current damper 2006 *J. of Vibration and Acoustics, Tranactions of the ASME* **128** Issue 3 pp 294-302
[10] Bae J et al. 2012 Vibration suppression of cantilever beam using magnetically tuned-mass-damper *J. of Sound and Vibration* **331** pp 5669-5684
[11] Bae J et al. 2014 Vibration suppression of a Large Beam Structure Using Tuned Mass Damper and Eddy Current Damping *Shock and Vibration Hindawi Publishing Corporation* **2014** ID893914
[12] Rohlfing J, Gardonio P and Elliot S J 2011 base impedance of velocity feedback control units with proof-mass electrodynamic actuators *J. of Sound and Vibration* **330** pp. 4661-4675

Acknowledgments

The authors gratefully acknowledge the European Commission for its support of the Marie Sklodowska-Curie program through the ITN EMVeM project (GA 315967).